Available online at www.sciencedirect.com
ScienceDirect
Journal of the European Ceramic Society 28 (2008) 2903–2914
www.elsevier.com/locate/jeurceramsoc

Synthesis of yttrium aluminum garnet (YAG) powder by homogeneous precipitation combined with supercritical carbon dioxide or ethanol fluid drying

Yang Ru *, Qin Jie, Li Min, Liu Guoqiang

State Key Laboratory of Chemical Resource Engineering, Beijing University of Chemical Technology, Beijing 100029, China

Received 20 February 2008; received in revised form 18 April 2008; accepted 13 May 2008
Available online 25 June 2008

Abstract

YAG precursors were synthesized by the urea method in aqueous solution using supercritical carbon dioxide and ethanol fluid drying technique, respectively. The composition of the precursors, the phase formation process and the properties of the calcined powders were investigated by means of XRD, IR, TG/DSC, BET, TEM and SEM. Compared with the classically prepared powders at room temperature in air, the amorphous precursor dried by supercritical CO_2 fluid was loosely agglomerated and directly converted to pure YAG at about 900 °C. The resultant YAG powders showed good dispersity with an average crystallite size about 20 nm and specific surface area of 52 $m^2\ g^{-1}$. However, the precursor dried by supercritical ethanol fluid was crystalline. Extensive phase segregation occurred during the drying process and resulted in the formation of separate phases such as monoclinic $Y(OH)_3$ and pseudoboehmite. YAM and YAP phases appeared in the calcination process and phase pure were not detected until 1200 °C.
Published by Elsevier Ltd.

Keywords: A1. Homogeneous precipitation; A2. Supercritical CO_2 fluid; A3. Supercritical ethanol fluid; D. YAG

1. Introduction

Yttrium aluminum garnet $Y_3Al_5O_{12}$ (YAG) exists in the cubic garnet structure and has a variety of good optical properties as well as excellent chemical stability and creep resistance.[1,2] Doping with other rare earth ions, such as Nd^{3+}, Ce^{3+} etc., into YAG makes it an ideal material for phosphors and solid-state lasers, which have attracted both technological and industrial interest.[3,4]

The single crystal YAG is normally synthesized by the Czochralski (CZ) method.[5] Unfortunately, YAG single crystals are very expensive, and it is difficult to produce large size YAG single crystals with high dopant concentrations. Recently, transparent polycrystalline YAG has attracted significant attention for its potential applications in high-power solid-state lasers.[6–8] Compared with the single crystal form, polycrystalline YAG ceramics have the advantages of low price, ease of manufacture and mass-production, the possibility of making large sized crystals with high dopant concentrations and so on. The laser characteristics of the Nd:YAG ceramics[9] were revealed to be nearly equivalent or superior to those of the high-quality Nd:YAG single crystal fabricated by Czochralski method. However, either for phosphor applications or high density and transparency polycrystalline YAG ceramics, highly dispersed and ultra-fine YAG powder is necessary. Traditional solid-state[10–12] synthesis of YAG powders from stoichiometric mixed yttria and alumina compounds requires a temperature higher than 1600 °C with a prolonged heating period and repeated mechanical mixing. Unfortunately, two intermediate phases YAP ($YAlO_3$, yttrium aluminum perovskite) and YAM ($Y_4Al_2O_9$, yttrium aluminum monoclinic) are produced during the heating period, and these processing conditions do not permit facile control of microstructure, grain size, grain size distribution, or shape of the resulting powders, leading to hard agglomeration and contamination of the powder. For correcting these drawbacks of the solid-state reaction process, many wet chemical methods have been developed and successfully used for powder

* Corresponding author. Tel.: +86 10 64436736; fax: +86 10 64436736.
E-mail address: yangru@bbn.cn (Y. Ru).

0955-2219/$ – see front matter. Published by Elsevier Ltd.
doi:10.1016/j.jeurceramsoc.2008.05.005

processing in recent years. These methods include sol–gel processing,[13–15] hydrothermal and solvothermal synthesis,[16–20] co-precipitation,[21–23] homogeneous precipitation,[24,25] spray pyrolysis,[26,27] and combustion.[28–30] These chemical processes achieve intimate mixing of reactant cations on the atomic level, leading to an increase in reaction rate and lowering synthesis temperature. Sol–gel method is the most widely employed chemical route to mixed metal oxides, and it has the apparent advantages of lower heat-treated temperature. However, it also has some disadvantages, such as the pH control, expensive starting materials and long reaction time, all of which have limited its mass-production. The hydrothermal and solvothermal synthesis of YAG powder can avoid the problems described above. However, hydrothermal synthesis requires complicated and expensive facilities due to the higher operating temperatures and pressures. Compared with these methods, homogeneous precipitation method is one of the most promising techniques because of the inexpensive starting materials, a simple synthesis process and commonly available apparatus. Urea has been successfully used as the precipitant, which provides the advantage of slow, uniform production of anionic species, e.g. OH^- and CO_3^{2-}, through the hydrolysis of its thermal decomposition products. However, the ultra-fine particles of the gel-like precursors underwent severe agglomeration during drying, causing poor sinterability of the resultant YAG powders. The cause is reported to be the surface tension of the water used as both the reagent and rinse solution.[31,32] Though special measures were taken during powder processing to alleviate agglomeration, the problem was not well solved. The best solution is the use of supercritical (SC) fluid which behaves as both a high-density gas and a diffusible liquid. Under supercritical conditions, there is essentially no gas/liquid interface, so the surface tension of SC fluid is zero. Therefore, supercritical fluid drying technique has been developed and successfully used for nanostructure fabrication such as TiO_2 and silica aerogels.[33,34]

In this study, for the first time, YAG precursor powders were synthesized by homogeneous precipitation combined with supercritical CO_2 and ethanol fluid drying technique, respectively. For comparison, conventional drying method in air at room temperature was also used. Phase evolution of the precursors and properties of the resultant YAG powders were investigated and compared among the three methods.

2. Experimental

The YAG precursor powders were synthesized using Y_2O_3 (99.999%), $Al(NO_3)_3{\cdot}9H_2O$ (99%), and urea (99%) as starting materials. Aqueous nitrate solution of Y^{3+} was prepared by dissolving Y_2O_3 in slightly excess nitric acid (99%) and some deionized water under heating and stirring. The $Al(NO_3)_3$ solution was prepared by dissolving $Al(NO_3)_3{\cdot}9H_2O$ in deionized water. The respective nitrate solutions with a cationic molar ratio for Y:Al of 3:5 were mixed in a container. Then the aqueous solution of urea was prepared and mixed with the nitrate solution while stirring. Next the solutions were hold at the temperature of 95 °C to form the precipitate. After aging, the precipitate was separated from the supernatant by centrifugation. The precursor precipitates were washed several times with distilled water to remove the byproducts of the precipitation reaction, such as NO_3^- and CO_3^{2-}. The resulting product was azeotropically distilled with absolute ethanol to remove the absorbed water and the hydrated water, and then divided into three portions that were separately dried as follows.

The first portion was conventionally dried in air at room temperature and the obtained precursor sample was labeled as Y–Al–air. For the second portion the ethanol in the product was extracted using supercritical carbon dioxide fluid. Literature[35] showed the extraction of alcohol with supercritical CO_2 should occur at conditions above the binary critical curve of CO_2 and the alcohol. At these conditions the alcohol and CO_2 are completely miscible. The prepared gel-like precursor sample with ethanol was carefully put into the extraction autoclave. Then liquid CO_2 pre-heated to 40 °C (above its critical temperature 31.1 °C) was pumped into the extractor to a pressure above 7.38 MPa. During drying, the flow of CO_2 to the autoclave was constant at 5–10 kg min^{-1}, and controlled independently of pressure. After circulating for 12 h, when the ethanol in the precursor was completely replaced by supercritical CO_2, the autoclave was rapidly depressurized to an atmospheric pressure and dried precursor powder was obtained, labeled as Y–Al–CO_2. A third precursor gel portion was dried using supercritical ethanol fluid. The precipitate was put into the autoclave. Then the autoclave was filled with ethanol and heated hermetically to a programmed temperature higher than 243 °C (the critical temperature of ethanol). The pressure was kept slightly above the critical pressure of ethanol (6.3 Mpa), and maintained for 30 min. After releasing the ethanol in the autoclave rapidly, the temperature was decreased to room temperature and dried precursor powder was obtained, labeled as Y–Al–ethanol.

The precursor powders prepared by the above three different drying method were then heat treated at varying temperatures from 800 to 1200 °C for 2 h at a heating rate of 5 °C min^{-1} in a muffle furnace under air atmospheres.

Phase identification of the samples heat-treated at different temperatures was performed by X-ray powder diffraction (XRD) pattern on a Japan Rigaku D/Max-2400 diffractometer, operated at 28 kV and 40 mA. The powders were ground and then loaded in sample holders for data collection, using Cu Kα radiation ($\lambda = 1.54178$ Å) and a scanning speed of 10° min^{-1}over a 2θ range of 10–90°. The products, their peak positions, and the relative intensities were characterized by comparing with standard JCPDS files. Particles size was estimated using the Scherrer equation on the XRD line-widths.

TEM pictures of the sintered powders were taken using a HITACHI H-800-1 transmission electron microscopy operated at 200 kV and images were observed at a magnification of 100,000×. The samples for electron microscopy were prepared by grinding in an agate mortar and subsequent dispersing the powder in ethanol. The suspension was treated in ultrasonic bath for about 10 min. A drop of very dilute suspension was applied on carbon-coated grid, which was then dried in air. SEM photographs were obtained using a HITACHI S-4700 scanning electron microscopy working at 20 kV, and samples were gold coated prior to analysis.

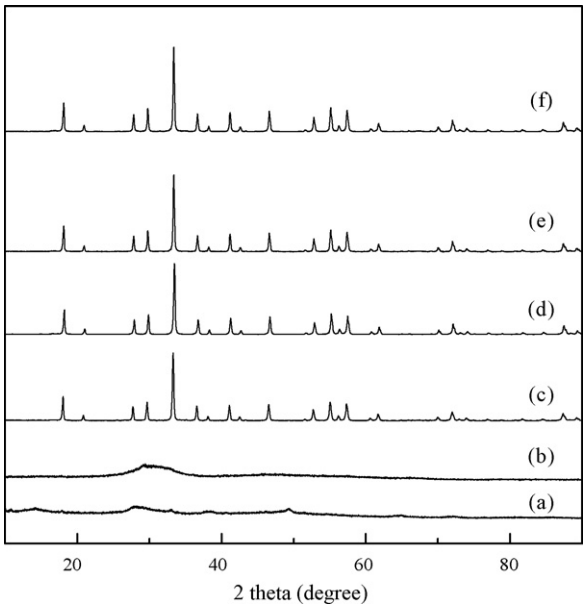

Fig. 1. XRD patterns of the precursor dried at room temperature and powders heated at different temperatures: (a) precursor, (b) 800 °C, (c) 900 °C, (d) 1000 °C, (e) 1100 °C, (f) 1200 °C.

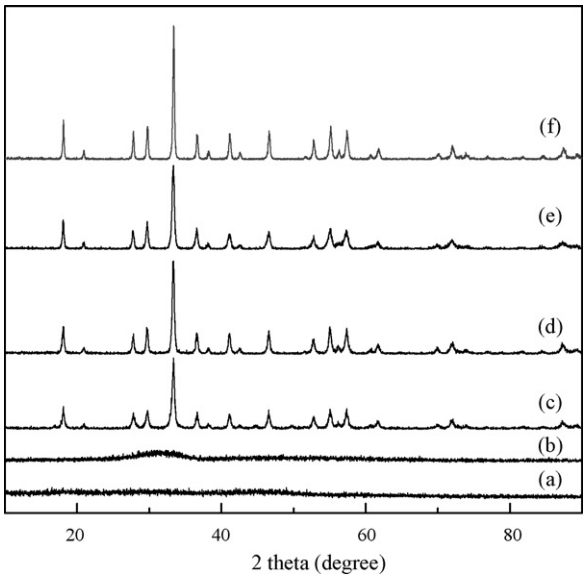

Fig. 2. XRD patterns of the precursor dried by supercritical CO_2 fluid technique and powders heated at different temperatures: (a) precursor, (b) 800 °C, (c) 900 °C, (d) 1000 °C, (e) 1100 °C, (f) 1200 °C.

Differential thermal and thermogravimetric analysis of YAG precursors were performed using a NETZSCH STA 449C TG/DSC analyzer from room temperature to 1400 °C. Approximately 5.00 mg of sample was loaded in an aluminum crucible and heated at 10 °C min^{-1} to 1400 °C under air atmospheres. The reference material was alpha-alumina.

FTIR spectra of the as-prepared precursor and the calcined powders were measured on a Nicolet 210 spectrophotometer in the 400–4000 cm^{-1} range using the KBr pellet method. Each analysis consisted of a minimum 32 scans and the resolution was $\pm 2\ cm^{-1}$.

Specific surface area analyses of the sintered powders were conducted at 77 K using an ASAP 2020 Micromeritics, with N_2 as the absorbate gas. Before determination of an adsorption isotherm, samples were degassed at 200 °C for 8 h. The specific surface areas were calculated using the BET multipoint method with eight data points.

3. Results

3.1. XRD results

Commercial YAG products were fabricated by a solid-state reaction method with long sintering time at high temperature and milling process because of high refractory properties of YAG. In the homogeneous precipitation method, phase pure YAG particles could be obtained at lower temperature than solid-state reaction methods because of the good mixing of each reactant in the order of several nanometers.[36] X-ray diffraction (XRD) patterns of the precursor dried at room temperature in air (Y–Al–air) and powders calcined at various temperatures between 800 and 1200 °C for 2 h are shown in Fig. 1. It can be seen that no sharp diffraction peaks are observed in samples calcined at temperature below 800 °C, and all the characteristic XRD peaks of YAG phase (JCPDS Card No. 33-40) appear when calcined at 900 °C. Further calcining at higher temperatures leads to the enhancement in the YAG diffraction peak intensity and reduces in the full-width at the half-maximum due to the improvement of crystallization and grain growth. Fig. 2 exhibits the XRD patterns of the precursor dried by supercritical CO_2 fluid (Y–Al–CO_2) and powders heat treated in the same temperature range of 800–1200 °C. Similar with Fig. 1, no peaks appear below 800 °C and YAG appears to crystallize directly from the amorphous precursor at 900 °C without the formation of any intermediate phase. The main difference between Fig. 1 and Fig. 2 is that the XRD patterns of YAG powders in Fig. 2 exhibit broader peaks than those of powders in Fig. 1, indicating the smaller microcrystal particles obtained from precursors dried by carbon dioxide supercritical fluid. The average crystallite sizes of the YAG powders derived from the precursors Y–Al–air and Y–Al–CO_2 at different calcination temperatures are calculated from the (4 2 0) XRD peak by X-ray line broadening using the Scherrer equation,[37] and the results are shown in Fig. 3. It can be seen that at same calcination temperatures, the average crystallite sizes of the YAG powders derived from precursor Y–Al–CO_2 are much smaller than those of powders from precursor Y–Al–air. The initially crystallized YAG powder from precursor Y–Al–CO_2 at 900 °C has an average crystallite size about 20 nm. Rapid crystallite growth was observed from 1100 °C for Y–Al–CO_2 samples and 1000 °C for Y–Al–air samples.

Fig. 4 shows the XRD pattern of the heat-treated YAG precursor powder obtained from supercritical ethanol fluid drying technique (Y–Al–ethanol). Obvious diffraction peaks of monoclinic $Y(OH)_3$ (JCPDS Card No. 21-1447) are observed in the XRD pattern of the precursor, but these diffraction peaks disappear when the precursor is calcined at 800 °C. With fur-

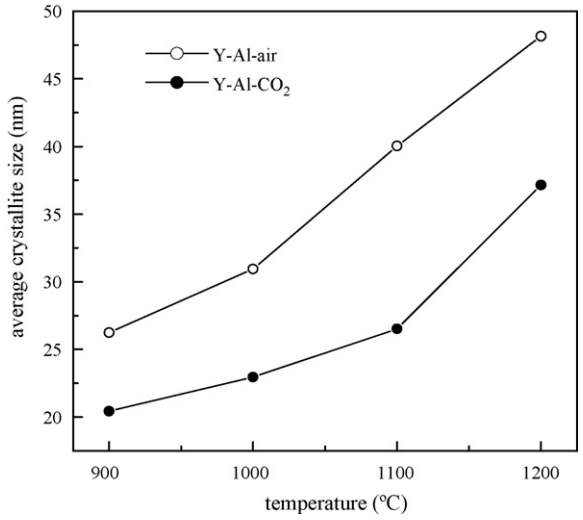

Fig. 3. Average crystallite sizes of the YAG powders derived from the precursors Y–Al–air and Y–Al–CO_2 at different calcination temperatures.

ther heating, main characteristic peaks of YAM phase (JCPDS Card No. 14-475) are observed at 900 °C with trace of YAG and hexagonal YAP (JCPDS Card No. 16-219). At 1000 °C, the amounts and intensity of YAG and YAP peaks are increased with loss of amount and intensity of YAM peaks. When the temperature is increased to 1100 °C, the amount and intensity of two intermediate phases YAM and YAP decrease while the amount and intensity of YAG phase increase. Pure YAG is not detected until the heating temperature comes up to 1200 °C.

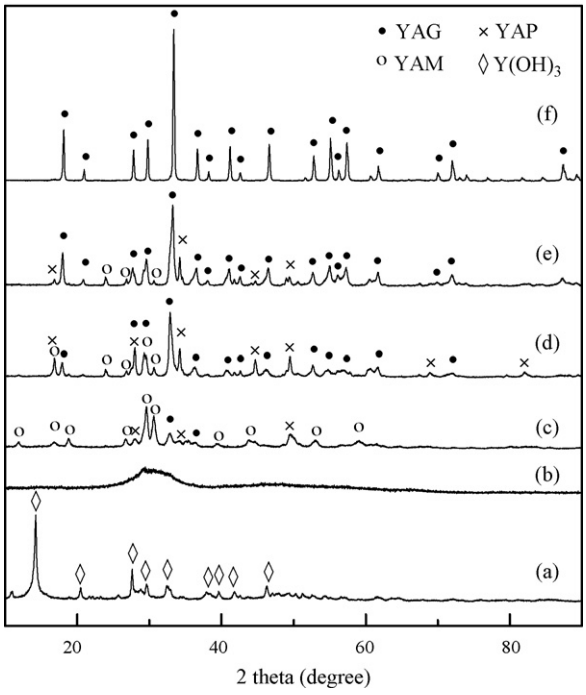

Fig. 4. XRD patterns of the precursor dried by supercritical ethanol fluid technique and powders heated at different temperatures: (a) precursor, (b) 800 °C, (c) 900 °C, (d) 1000 °C, (e) 1100 °C, (f) 1200 °C.

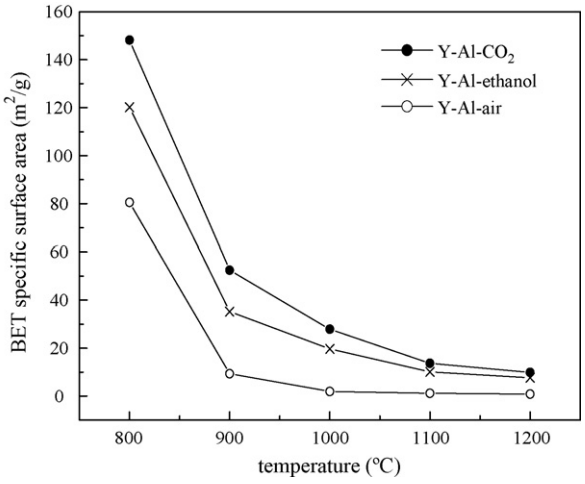

Fig. 5. BET surface area data of the precursor powders calcined at various temperatures.

3.2. Specific surface areas

The BET surface area data of the precursor powders calcined at various temperatures are shown in Fig. 5. It can be seen that YAG powders from the precursor dried by supercritical CO_2 show the highest BET surface areas among the three samples. The initially crystallized YAG powder from precursor Y–Al–CO_2 at 900 °C has a specific surface area as high as 52 m^2/g. BET surface areas of all the powders decrease rapidly with increasing calcination temperature. The reason for the decrease of specific surface area is that in the process of calcining, substances diffuse on the microcrystallite surface and inside microcrystallite mainly by surface diffusion, and the reaction driving force is the decrease of free surface energy of particles.[38] For two particles contacting each other both having large surface energy, the substances inside them move and the surface energy decreases when heated to below their melting point to make the two particles melt together and the particle size increase, leading to a decrease of specific surface area.[39]

3.3. IR spectroscopy

IR analysis of the synthesized samples was performed to gain more insight into the structure and composition of the amorphous powders. Fig. 6 shows the IR spectra of precursors and powders from them. It can be seen that the IR spectra of the two precursors Y–Al–air and Y–Al–CO_2 are almost the same. The broad absorption around 3400 cm^{-1} can be assigned to stretching vibration of hydroxyl bands (O–H) and 1630 cm^{-1} to O–H bands of the crystal water and absorbed water.[40] Absorption bands at about 1520 and 1380 cm^{-1} correspond to the characteristic asymmetrical split stretching of carbonates, indicating the presence of CO_3^{2-}.[41] The weak bands at 840 and 740 cm^{-1}, which are associated with the out-of-plane bending of CO_3^{2-},[42] further confirm the presence of the carbonate. The broad band in the region of 490–700 cm^{-1} should be assigned to the bending of A1–OH and Y–OH.[42] The weak peaks at about 2930 and 2850 cm^{-1} correspond to the vibrations of $–CH_2–$ and $–CH_3$,[32]

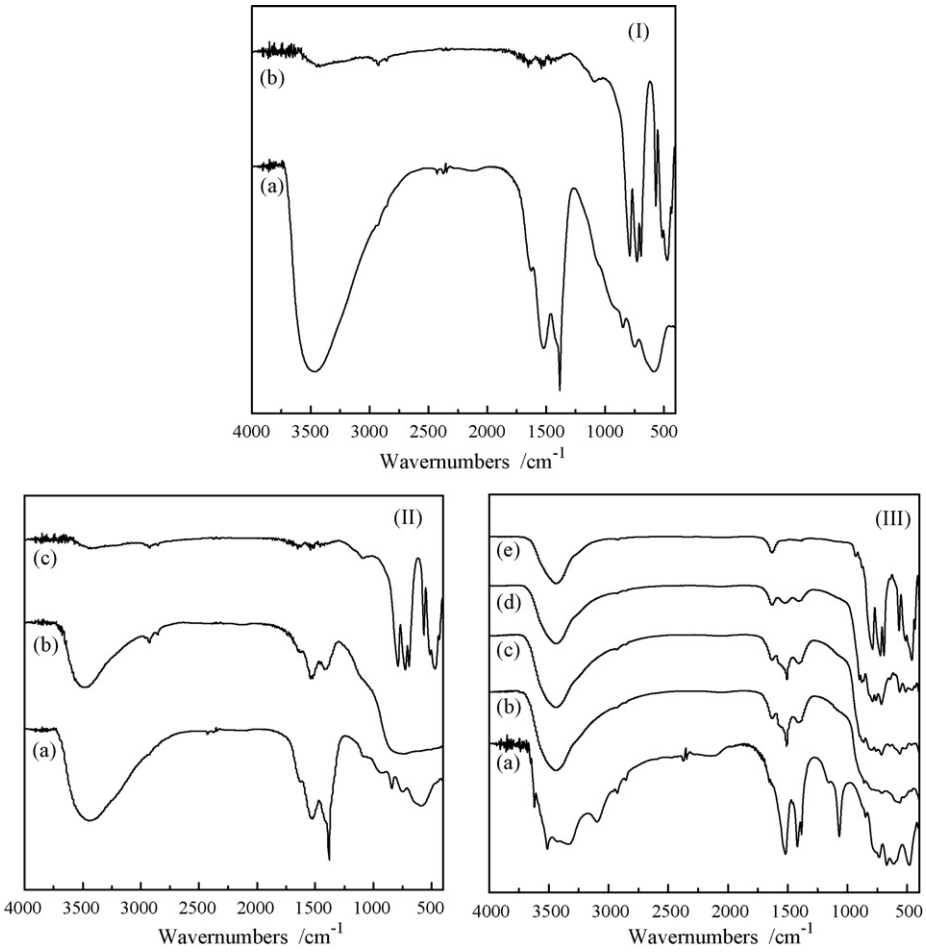

Fig. 6. IR spectra of precursors and that heated at different temperatures: (I) dried at room temperature: (a) precursor, (b) 1200 °C; (II) dried by supercritical CO_2 fluid technique: (a) precursor, (b) 800 °C, (c) 1200 °C; (III) dried by supercritical ethanol fluid technique: (a) precursor, (b) 800 °C, (c) 900 °C, (d) 1000 °C, (e) 1200 °C.

which reveals the presence of $–OC_2H_5$ groups. As temperature increases all the above peaks become weaker and finally disappear because of the decomposition of the precursor. At 1200 °C, new bands appear in the range 450–800 cm^{-1} (at 796, 720, 460 cm^{-1}), which in accord with earlier reports[19] are characteristic metal–oxygen (M–O) vibrations of YAG structure. This result can also be confirmed by XRD patterns shown in Figs. 1–2. The IR spectra of the precursor dried by supercritical ethanol and powders calcined at various temperatures are shown in Fig. 6(III). Besides the bands mentioned in Fig. 6(I–II), the absorption peaks at 3618, 3513 and 3425 cm^{-1} correspond to the stretching vibration of O–H in the monoclinic $Y(OH)_3$.[43] The intensity of the band at 1520 cm^{-1} is stronger than that in Fig. 6(I–II), this may be because the monoclinic $Y(OH)_3$ also reveals the bending vibration of O–H at 1520 cm^{-1} according to previous work.[43] The peaks at 3336, 3097 and 1068 cm^{-1} are assigned to the stretching and bending mode of O–H bands in pseudoboehmite,[44] which refer to the poorly crystallized Al^{3+} compound of composition $Al_2O_3{\cdot}nH_2O$ $(2.0 > n > 1.0)$.[45] All these peaks disappear when the precursor is calcined at 800 °C, indicating the precursor structure was destroyed. But all samples show intensive O–H vibration band even after they were calcined at higher temperatures. This may be caused by the absorption of H_2O in air, which was also observed in earlier studies.[41]

3.4. TG/DSC

The mechanism of the thermal decomposition of the three YAG precursors was studied by TG/DSC analyses as shown in Fig. 7a–c. The precursor dried at room temperature and dried by supercritical CO_2 present similar TG and DSC curves. The total weight losses shown in Fig. 7a and b are both found to be around 45%, indicating the two precursors may have the same composition. Much of the weight loss takes place up to 500 °C, which can be attributed to the removal of molecular water and decomposition of partial carbonates and hydroxides contained in the precursor. The DSC traces display a broad endothermic centered around 115 °C that is likely to correspond to the release of water. The small exothermic peak at about 380 °C observed in Fig. 7a and b, respectively, is probably due to the combustion of decomposed residual ethanol.[46] Because no weight loss is detected, the exothermic peaks at 963 °C in Fig. 7a and 935 °C in Fig. 7b are presumed to be caused by the crystallization of YAG. While the XRD patterns (see Figs. 1 and 2) show the crystallization of YAG

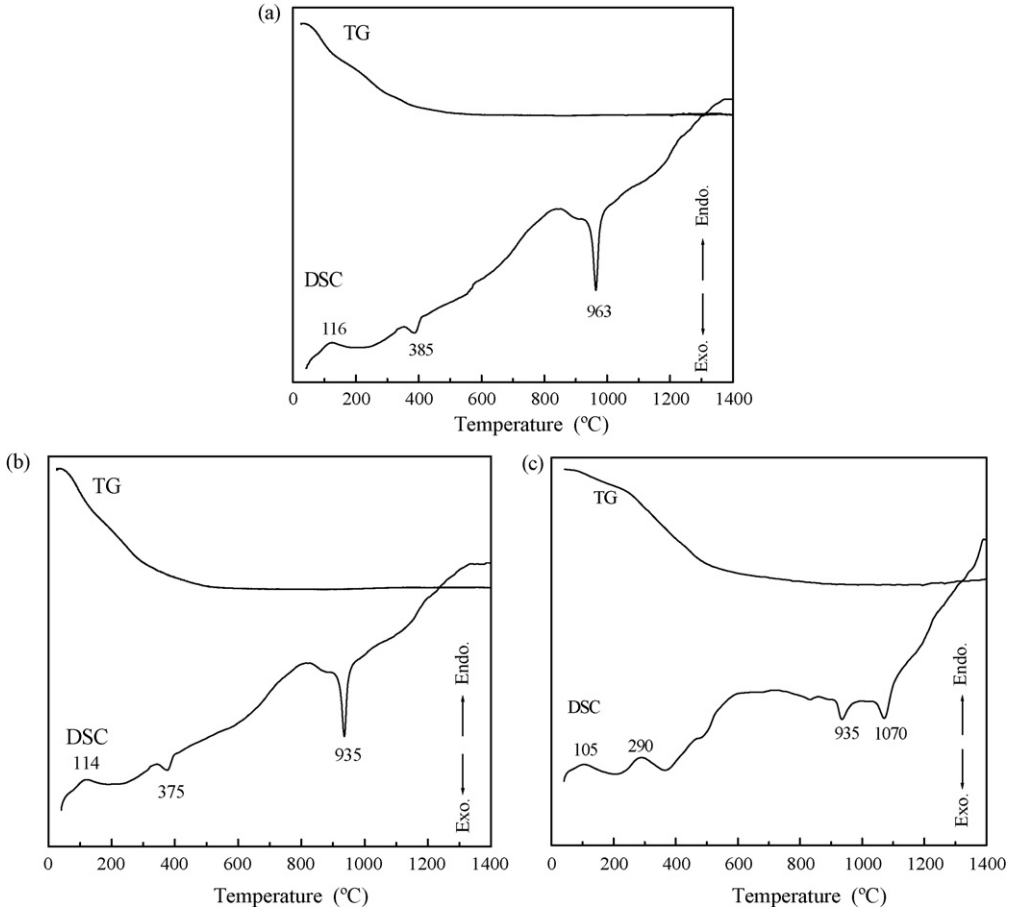

Fig. 7. TG/DSC curves of the precursors: (a) dried at room temperature; (b) dried by supercritical CO_2 fluid technique; (c) dried by supercritical ethanol fluid.

began below the temperature, because the exothermic peak in the DSC curve often lags after the crystallization.[36]

The TG curve of precursor dried by supercritical ethanol in Fig. 7c gives a total weight loss of 24.5%, which nears the weight loss of Y–Al–air or Y–Al–CO_2 in the temperature range of 240–600 °C. The DSC curve of precursor dried by supercritical ethanol consists of two endothermal peaks at 25–1200 °C. The initial weight loss would then correspond to two processes. The first process with an endothermic peak at 110 °C is due to dehydration of absorbed moisture in the powder. The second process with an endothermic peak at 290 °C may be due to the dehydration of pseudoboehmite. At temperature above 800 °C, no weight loss is detected and two clear exothermic peaks appear. The exothermic peak at 935 °C was caused by the crystallization of both YAM and YAP, as evidenced by the XRD patterns in Fig. 4. The peak at 1070 °C corresponds to YAM and YAP reacting with a polymorph of Al_2O_3 to form YAG by the reaction[24]: $2YAlO_3 + Y_4Al_2O_9 + 3\eta\text{-}Al_2O_3 \rightarrow 2Y_3Al_5O_{12}$. The diffraction peaks corresponding to η-Al_2O_3 are not observed in the XRD patterns, probably because of their very weak intensity compared with the large peaks of YAG.

3.5. Morphology

Fig. 8 shows SEM photographs of precursor dried at room temperature and YAG powders calcined at different temperatures between 900 and 1200 °C. The resultant powders, at any calcination temperature, are severely agglomerated and show similar overall morphology to that of the precursor. It is obvious that hard agglomerate structure of the precursor has retained to the calcined powders. Fig. 9 shows SEM morphologies of the powders calcined at various temperatures from the precursor dried by supercritical CO_2. The particles are monosized, spherical and less agglomerated. Though the grain sizes increase with increasing calcination temperature, relatively good dispersity persist. TEM photographs of precursor dried by supercritical ethanol and powders calcined at various temperatures shown in Fig. 10 consist of two kinds of morphologies. The first possesses a normal particle structure and the second type possesses a fiber shape. The fiber shape is very similar to the morphology of pseudoboehmite, which has a typical fibrillar particle shape.[45]

4. Discussion

4.1. Sequential precipitation processes

The present reaction solution system consists of $Y(NO_3)_3$, $Al(NO_3)_3$, and urea; the molar ratio of $[Y^{3+}]$:$[Al^{3+}]$ is 3:5 and the primary molar ratio of [urea]: $[Y^{3+} + Al^{3+}]$ is 6.0. The concurrent temperature and pH rise of the precipitation experiment are shown in Fig. 11. The pH decreased from an initial value of

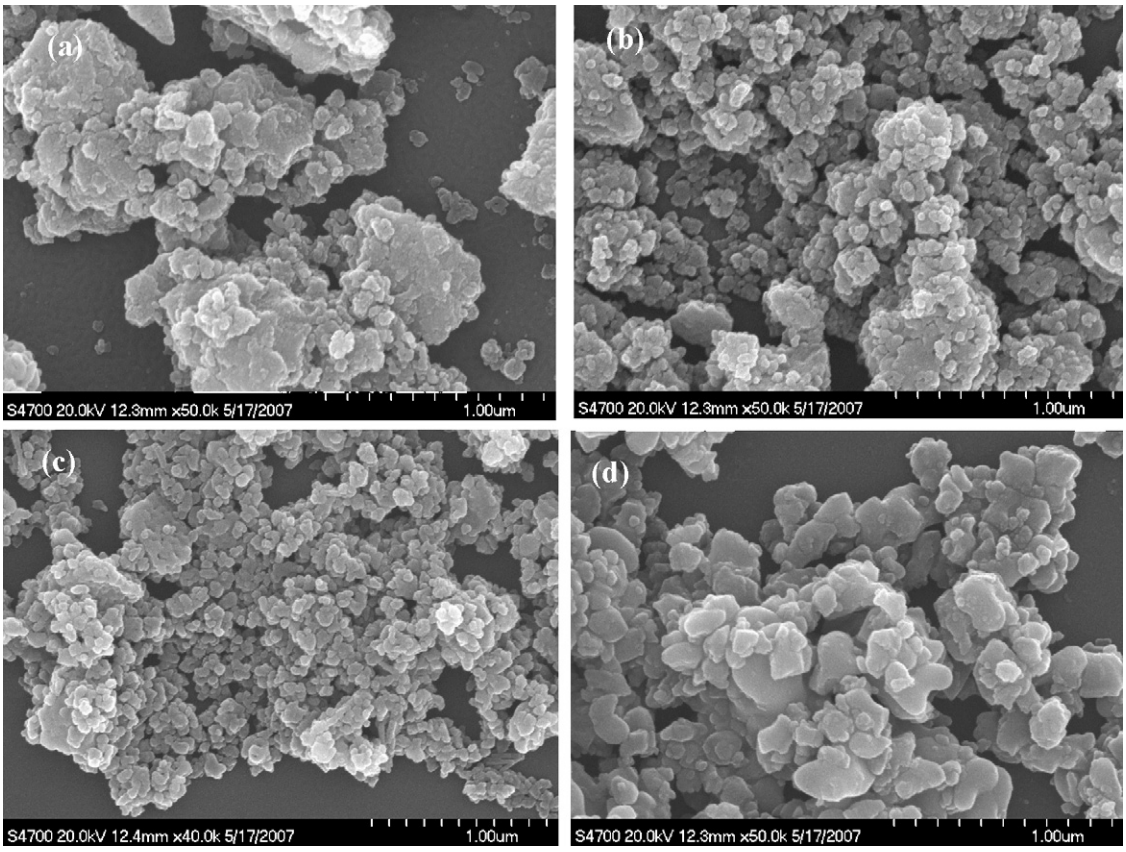

Fig. 8. SEM morphologies of the powders dried at room temperature: (a) precursor, (b) calcined at 900 °C, (c) 1000 °C, (d) 1200 °C.

2.90 to its lowest point of 2.84. Turbidity was observed in this clear solution when the pH value increased to about 3.5, and maintained for some time. Then the pH rapidly increased to 5.0 and later showed a distinct plateau around 6.0. The pH rise is due to the decomposition of urea and subsequent hydrolysis of the products. The pH plateau is contributed to precipitation reactions. The controlled hydrolysis of urea results in either CO_2 in acidic medium or to CO_3^{2-} in basic medium as shown below[47]:

$$H_2N\text{–}CO\text{–}NH_2 \rightarrow NH_4^+ + OCN^- \quad (1)$$

$$OCN^- + 2H^+ + H_2O \rightarrow CO_2 + NH_4^+ \quad (2)$$

$$OCN^- + OH^- + H_2O \rightarrow NH_3 + CO_3^{2-} \quad (3)$$

Along with the temperature increases, more and more urea hydrolyzes and the consumption of H^+ results in the increase of pH in the solution, and precipitations of metal cations occur during this process. Previous works have reported that the homogeneous precipitation by urea method in nitrates solutions is sequential[24,25]: aluminum ions precipitated first, followed by the yttrium ions which precipitated onto the aluminum compound particles to produce fine YAG precursor precipitates. However, the sequential precipitation in those works was mainly confirmed by experiments and characterizations, no reason was given to explain why the precipitation is sequential. In this paper the sequential precipitation process is investigated by calculating the precipitation pH of metal cations using solubility product principle. The essential reason for the sequential precipitation will be found to be the difference in solubility products of indissoluble compounds.

In the precipitation process, turbidity was first observed at pH about 3.5. Under this pH condition, the cyanate ions generated by urea decomposition is converted into carbon dioxide via Eq. (2) and the main precipitants were hydroxyl ions, so the precipitates should be hydroxides. The solubility products (K_{sp}) of amorphous $Al(OH)_3$ and $Y(OH)_3$ are 1.3×10^{-33} and 8.0×10^{-23}, respectively.[48] Combined with the concentrations of aluminum ions and yttrium ions in the reaction solution it can be calculated that the precipitation pH of $Al(OH)_3$ and $Y(OH)_3$ are 3.3 and 6.9, respectively. So the first pH plateau around 3.5 in Fig. 11 is caused by the formation of $Al(OH)_3$:

$$Al^{3+} + 3OH^- \rightarrow Al(OH)_{3(s)} (K_{sp} = 1.3 \times 10^{-33}) \quad (4)$$

This is consistent with the results of literature,[49] in which aluminum hydroxides were obtained by urea method at a pH of 3.6. Work in literature[24] also reported that the main aluminum component of the precipitate was aluminum hydrate. The precipitation reaction of $Al(OH)_3$ is hydroxyl consuming, so the urea hydrolysis equilibrium (1) is displaced towards the end-products and more and more urea hydrolyzes. After the pH plateau at 3.5 the system pH value rapidly increases to 5.0, and another pH plateau appear at a value of 6.0. Previous work[25] has confirmed that nearly all of the aluminum ions had

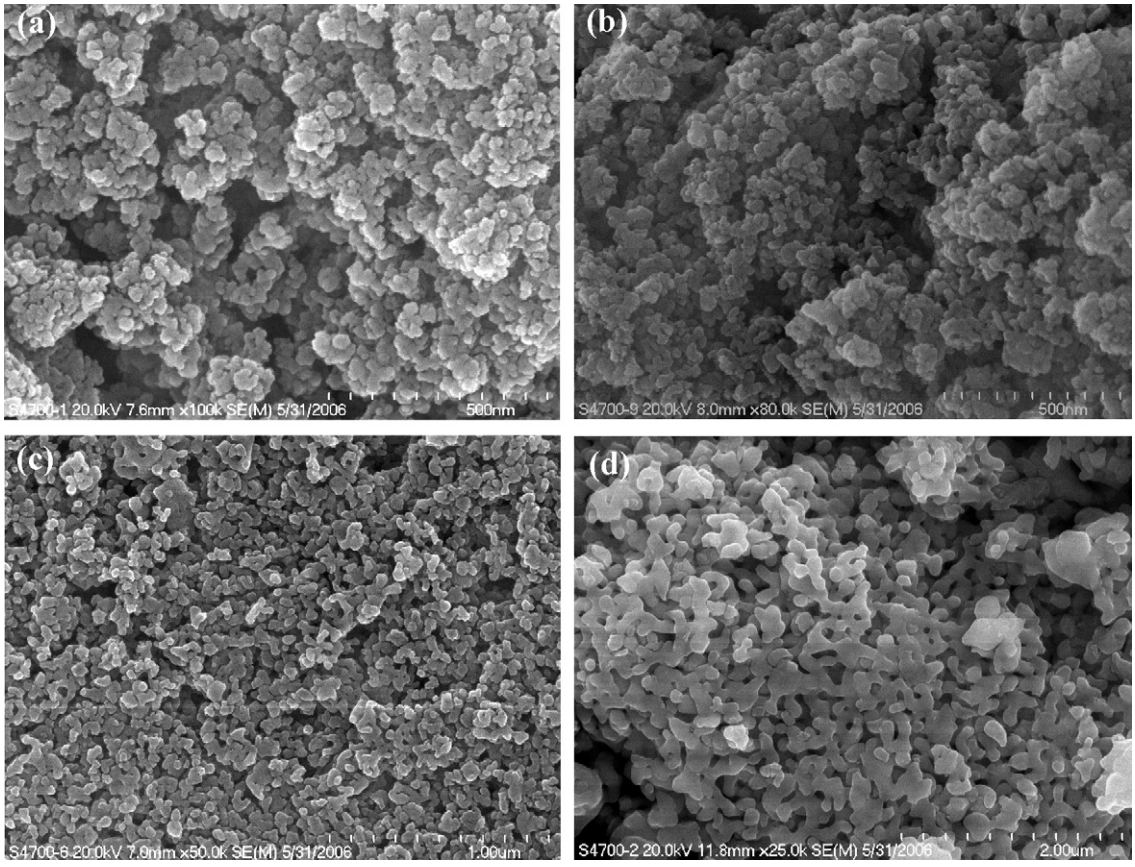

Fig. 9. SEM morphologies of the powders synthesized with supercritical CO_2 fluid drying technique: (a) powders calcined at 800 °C, (b) 900 °C, (c) 1000 °C, (d) 1200 °C.

precipitated when a visible solid phase appeared, so the second pH plateau around 6.0 should correspond to the precipitation of yttrium compounds. However, the pH value is lower than the precipitation pH of $Y(OH)_3$. The calculation of precipitation pH using solubility products indicates $Y(OH)_3$ precipitates at pH 6.9, and work in literature[50] has also reported the precipitation of $Y(OH)_3$ occurred at a pH of 6.8. This observation suggests that the precipitate of yttrium compounds produced around pH 6.0 is more complex than a simple hydroxide. Notice that the increase of pH has driven the equilibrium reaction (3) to the right hand side to generate CO_3^{2-}. According to the fact that the solubility product[51] of $Y_2(CO_3)_3$ is equal to 2.5×10^{-31}, it can be thought that $Y_2(CO_3)_3$ precipitate will be produced when the concentration of CO_3^{2-} reaches 2.9×10^{-10} M under the present experimental conditions. It can be calculated through equilibrium reaction (3) that this concentration of CO_3^{2-} corresponds to a pH higher than 4.5. In addition, previous study[52] on urea hydrolysis in aqueous solution has investigated the species distribution as a function of the pH value, and their results revealed that the concentration of CO_3^{2-} could reach 2.9×10^{-10} M at a pH slightly lower than 6.0. So yttrium carbonates may begin to precipitate at a pH between 4.5 and 6.0. It can be seen that the pH curve in Fig. 11 shows a slow increase from 5.0 to 6.0, so it is probably due to the formation of $Y_2(CO_3)_3$ through the following reaction:

$$2Y^{3+} + 3CO_3^{2-} \rightarrow Y_2(CO_3)_{3(s)} (K_{sp} = 2.5 \times 10^{-31}) \quad (5)$$

This reaction is hydroxyl consuming indirectly, so the urea hydrolysis equilibrium (1) is also displaced towards the end-products to make more urea hydrolyze. When the system pH reaches 6.0, yttrium basic carbonate would precipitate from the solution[53]:

$$Y^{3+} + OH^- + CO_3^{2-} \rightarrow YOHCO_3 \quad (6)$$

This is the reason that the pH curve shows a plateau at the value around 6.0 as shown in Fig. 11. After that, the pH value rises slowly to higher than 7.0, and in this process yttrium hydroxides may or may not form. If the final pH reaches as high as the precipitation pH of $Y(OH)_3$ and there are still Y^{3+} ions left in the solution after reactions (5) and (6), yttrium hydroxides will form through the following reaction:

$$Y^{3+} + 3OH^- \rightarrow Y(OH)_{3(s)} (K_{sp} = 8.0 \times 10^{-23}) \quad (7)$$

In fact, yttrium hydroxides are contained in the precursor precipitates, as confirmed by the XRD patterns in Fig. 4. So the yttrium compounds are considered to be a mixture of hydrated carbonates, hydrated basic carbonates, and hydrated hydroxides. This is consistent with earlier work[54] in which europium-doped yttrium oxide phosphors were prepared via urea precipitation, and amorphous carbonates and amorphous hydroxides/carbonates mixtures were identified as precursors from ethanol and ethylenediamine, respectively.

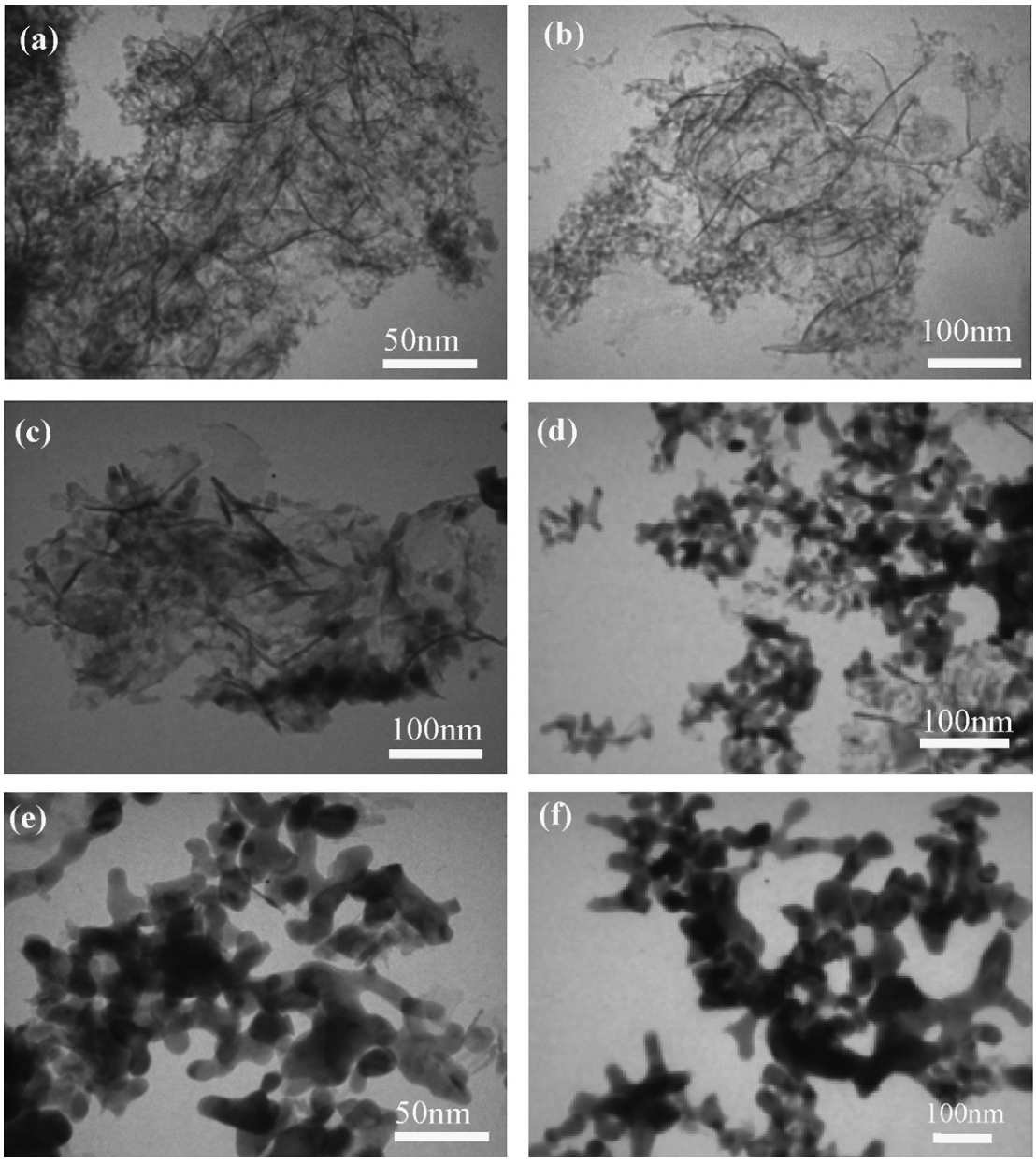

Fig. 10. TEM micrographs of powders calcined at various temperatures from the precursor dried by supercritical ethanol fluid: (a) precursor, (b) calcined at 800 °C, (c) 900 °C, (d) 1000 °C, (e) 1100 °C, (f) 1200 °C.

In conclusion, the sequential precipitation reaction in the mixed aqueous solution of $Y(NO_3)_3$, $Al(NO_3)_3$, and urea is determined by the difference in solubility products. Composition of the precursor will be the result of competition between OH^- and the carbonate species generated by the hydrolysis reactions of urea during combining with metal cations. This situation is similar in some extent with the co-precipitation system by NH_4HCO_3 method,[55] in which OH^- and the carbonate species generated by NH_4HCO_3 compete to combine with metal cations to produce a carbonate-type precursor precipitate. In the precipitation of aluminum ions, hydroxide ions generated by decomposition of urea play a critical role, and the precipitates are mainly hydrated aluminum hydroxides; while in the followed precipitation of yttrium ions, carbonate ions generated by the urea decomposition control the precipitation, and the yttrium precipitates may consist of hydrated carbonates, hydrated basic carbonates, and hydrated hydroxides. The general formula of the YAG precursor precipitate may roughly be expressed as $Y_3Al_5(OH)_{24-2x}\cdot(CO_3)_x\cdot nH_2O$, which is consistent with literature.[25]

4.2. Effects of drying methods on reaction sequences of precursors

The XRD patterns in Fig. 1 reveal that the precursor dried at room temperature was amorphous and the infrared spectrum in Fig. 6(I) shows the presence of hydroxyl groups and carbonate. The TG curve in Fig. 7(a) gave a total weight loss of 45%, which

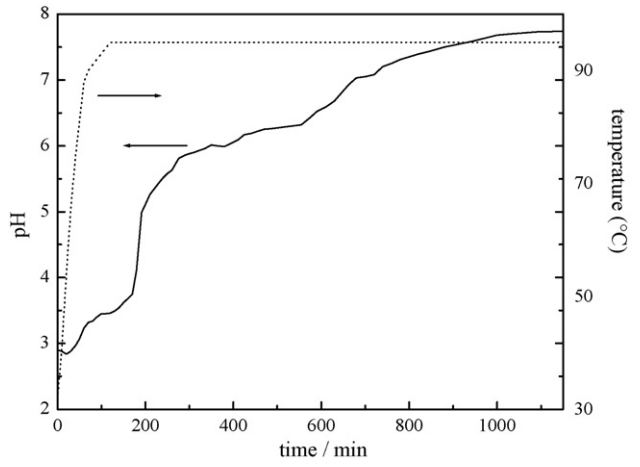

Fig. 11. Changes of pH and temperature with time under [U]/[M] ratio of 6.

is too high for a simple hydroxide. All those results indicate that the precursor precipitates dried at room temperature are mixtures of hydrated hydroxides and carbonates/basic carbonates with a general formula of $Y_3Al_5(OH)_{24-2x}\cdot(CO_3)_x\cdot nH_2O$. Both the XRD patterns in Fig. 1 and DSC curve in Fig. 7(a) showed that pure YAG is formed from such a precursor without any other intermediate phase, indicating high cation homogeneity of the precursor.

A comparison between the XRD patterns, IR spectrums, and TG-DSC curves of Y–Al–air and Y–Al–CO_2 samples shows that the precursor dried by supercritical carbon dioxide fluid seems to have the same composition as the precursor dried at room temperature and undergo similar reaction sequences during the thermal decomposition. Combined with the BET surface area data in Fig. 5 and SEM photographs in Figs. 8 and 9, it can be concluded that CO_2 supercritical drying technique has greatly improved the dispersity of the precursor powder without changing its composition and structure. YAG crystallized directly from the amorphous precursor without the formation of any intermediate phase. This result is different from that of the traditional solid-state reaction method, in which YAP ($YAlO_3$) and/or YAM ($Y_4Al_2O_9$) usually appeared as intermediate phases.[56] It is reported that the initial formation of YAM from aluminum and yttrium oxide and the subsequent formation of YAP rather than YAG are both consistent with phase formation order controlled by diffusion of Al and O, with relative immobility of Y.[57] The direct formation of YAG in this work indicate the diffusion length from Al and O to relatively immovable Y was shortened. It can be conjectured that the sequential precipitation process has produced a core–shell structure which has an yttrium compounds shell surrounding an aluminum compounds core. The precursors with such a structure are of good intimate atomic mixing and have a Y:Al proportion equal to the 3:5 ratio in which they were combined in the precursor synthesis. So pure YAG was formed directly in the calcination process because of the proper Y:Al ratio of 3:5 and the shortened diffusion length.

The reaction sequences that explain the crystallized products after calcinations at various temperatures for the precursor dried by supercritical ethanol fluid are complicated. XRD patterns in Fig. 4 and DSC curve in Fig. 7(c) reveal the formation of YAM and YAP as well as YAG, and phase pure YAG is not detected until 1200 °C. The different phase formation order of the precursor Y–Al–ethanol may be caused by the changes in its composition and structure. Both the XRD patterns in Fig. 4 and the infrared spectrum in Fig. 6(III) reveal that the precursor Y–Al–ethanol contains monoclinic $Y(OH)_3$, and the infrared spectrum also shows the presence of pseudoboehmite, which refers to the poorly crystallized Al^{3+} compound of composition $Al_2O_3\cdot nH_2O$ ($2.0 > n > 1.0$) with a typical fibrillar particle shape.[45] The total weight loss in Fig. 7(c) is 24.5%, indicating that the composition is different from that of precursor Y–Al–air and Y–Al–CO_2. The essential reason for these changes in composition and structure may be temperature. In supercritical ethanol drying process the temperature is 250 °C, much higher than the temperature of CO_2 supercritical drying process (40 °C). The rather high temperature will supply energy for the phase transition of amorphous $Y(OH)_3$ and dehydration of the fresh precipitate. Monoclinic yttrium hydroxide was once prepared hydrothermally from amorphous yttrium hydroxide at 300 °C.[43] In addition, CO_2 supercritical drying was a dynamic circulation process, and the liquid CO_2 was pre-heated to 40 °C before it was pumped into the autoclave, so the heat transfer was homogeneous. But in supercritical ethanol drying process ethanol in the autoclave was static and the system was heated hermetically from a room temperature to a programmed temperature, so the heat transfer was non-homogeneous and temperature gradient may be generated. It is likely that segregation of the precursors occurred under such conditions and result in the formation of separate phases such as monoclinic $Y(OH)_3$ and pseudoboehmite. Extensive phase segregation caused by temperature was also observed in the spray pyrolysis experiments, and their results suggest that the formation of phase-segregated powders as intermediate phases does not enable the formation of the garnet phase.[58] Apparently the homogeneous mixture with a core–shell structure described above has been destroyed by the phase segregation and the local Y:Al ratio of the oxide products does not match the stoichiometric ratio of YAG, which finally results in the formation of kinetically stable phase such as YAM and YAP as well as the target thermodynamically stable phase YAG.[58] In situations where segregated phase appear, subsequent reaction is needed at higher temperatures to produce garnet.[57]

4.3. Formation and the elimination of agglomeration

One of the important steps during powder synthesis using the precipitation procedure is the drying of the wet precipitates. Many important powder properties, for example: the homogeneity, the size of the agglomerates and the extent of agglomeration are developed during this important step of powder synthesis.[59] If the precursor precipitates were dried by evaporating liquid media, comparatively hard agglomerates would occur among the powders by the capillary attraction because of the existence of the liquid to vapor phase transformation of liquid media.[60] It can be seen in Fig. 8 that the YAG precursor powders conventionally dried by evaporating water and ethanol used as the washing solvent was strongly

agglomerated, which is usually harmful to applications of materials and should be avoid.

In supercritical-fluid drying, compounds are heated and pressurized above their critical pressure and temperature, at which point liquid and vapor states become indistinguishable to form a fourth, supercritical fluid state with properties intermediate between liquid and gas. High supercritical densities (comparable to organic solvents) are sufficient to provide good solvent capability, but low enough for high diffusivity.[61] The solvent is removed in the supercritical state and the influence of surface tension does not exist because the gas–liquid interface does not exist, so ultrafine and soft-agglomerated particles can be obtained.[60,62] It can be seen in Fig. 9 that the supercritical CO_2 fluid treated powders show much better dispersity than the powders from conventional dried precursor. In addition, the resultant YAG powders from the supercritical fluid treated precursors display much higher specific surface areas (Fig. 5). All those results reveal that the agglomeration has been greatly reduced by supercritical fluid drying technique.

5. Conclusion

YAG precursor precipitates were obtained via homogeneous precipitation from a mixed solution of aluminum and yttrium nitrates using urea as the precipitant. The difference in solubility products of yttrium compounds and aluminum compounds is the essential reason for a sequential precipitation which produced an amorphous precursor of good atomic mixing. After conventionally dried in air at room temperature the precursor was severely agglomerated. In comparison, the amorphous precursor produced by supercritical CO_2 drying process was loosely agglomerated. After calcination it directly converted to pure YAG at about 900 °C without the formation of any intermediate phase and the resultant YAG powders showed the highest BET surface areas and the smallest crystallite sizes between the three samples. The precursor produced by supercritical ethanol drying process was crystalline. The high temperature during the supercritical ethanol drying process caused extensive phase segregation and resulted in the formation of separate phases such as monoclinic $Y(OH)_3$ and pseudoboehmite. When calcined the precursor transformed to pure YAG at about 1200 °C via YAM and YAP phases.

References

1. Harada, Y., Suzuki, T., Hirano, K., Nakagawa, N. and Waku, Y., Environmental effects on ultra-high temperature creep behavior of directionally solidified oxide eutectic ceramics. *J. Eur. Ceram. Soc.*, 2005, **25**, 1275–1283.
2. Yagi, H., Yanagitani, T., Numazawa, T. and Ueda, K., The physical properties of transparent $Y_3Al_5O_{12}$ elastic modulus at high temperature and thermal conductivity at low temperature. *Ceram. Int.*, 2007, **33**, 711–714.
3. Lu, J., Ueda, K., Yagi, H., Yanagitani, T., Akiyama, Y. and Kaminskii, A. A., Neodymium doped yttrium aluminum garnet ($Y_3Al_5O_{12}$) nanocrystalline ceramics—a new generation of solid state laser and optical materials. *J. Alloys Compd.*, 2002, **341**, 220–225.
4. Li, X., Li, Q., Wang, J. Y. and Yang, S. L., Synthesis of YAG:Eu phosphors with spherical morphology by solvo-thermal method and their luminescent property. *Mater. Sci. Eng.*, 2006, **B131**, 32–35.
5. Ikesue, A., Polycrystalline Nd:YAG ceramics lasers. *Opt. Mater.*, 2002, **19**, 183–187.
6. Strek, W., Bednarkiewicz, A., Hreniak, D., Mazur, P. and Lojkowski, W., Fabrication and optical properties of transparent Nd^{3+}: YAG nanoceramics. *J. Lumin.*, 2007, **122/123**, 70–73.
7. Kokta, M., Growth of oxide laser crystals. *Opt. Mater.*, 2007, **30**, 1–5.
8. Ikesue, A., Aung, Y. L., Yoda, T., Nakayama, S. and Kamimura, T., Fabrication and laser performance of polycrystal and single crystal Nd:YAG by advanced ceramic processing. *Opt. Mater.*, 2007, **29**, 1289–1294.
9. Lu, J., Prabhu, M., Xu, J., Ueda, K., Yagi, H., Yanagitani, T. *et al.*, Highly efficient 2% Nd: yttrium aluminum garnet ceramic laser. *Appl. Phys. Lett.*, 2000, **77**, 3707–3709.
10. Li, J., Wu, Y. S., Pan, Y. B. and Guo, J. K., Fabrication of Cr^{4+}, Nd^{3+}:YAG transparent ceramics for self-Q-switched laser. *J. Non-Cryst. Solids*, 2006, **352**, 2404–2407.
11. Ikesue, A. and Kinoshita, T., Fabrication and optical properties of high-performance polycrystalline Nd:YAG ceramics for solid-state lasers. *J. Am. Ceram. Soc.*, 1995, **78**, 1033–1040.
12. Alkebro, J., Colin, S. B., Mocellin, A. and Warren, R., Mechanical alloying of alumina-yttria powder mixtures. *J. Eur. Ceram. Soc.*, 2000, **20**, 2169–2174.
13. Lu, C. H., Hsu, W. T., Dhanaraj, J. and Jagannathan, R., Sol–gel pyrolysis and photoluminescent characteristics of europium-ion doped yttrium aluminum garnet nanophosphors. *J. Eur. Ceram. Soc.*, 2004, **24**, 3723–3729.
14. Sun, Z. H., Yuan, D. R., Li, H. Q., Duan, X. L., Sun, H. Q., Wang, Z. M. *et al.*, Synthesis of yttrium aluminum garnet (YAG) by a new sol–gel method. *J. Alloys Compd.*, 2004, **379**, L1–L3.
15. Fedyk, R., Hreniak, D., Łojkowski, W., Stręk, W., Matysiak, H., Grzanka, E. *et al.*, Method of preparation and structural properties of transparent YAG nanoceramics. *Opt. Mater.*, 2007, **29**, 1252–1257.
16. Hreniak, D., Fedyk, R., Bednarkiewicz, A., Stręk, W. and Łojkowski, W., Luminescence properties of Nd:YAG nanoceramics prepared by low temperature high pressure sintering method. *Opt. Mater.*, 2007, **29**, 1244–1251.
17. In, J. H., Lee, H. C., Yoon, M. J., Lee, K. K., Lee, J. W. and Lee, C. H., Synthesis of nano-sized YAG:Eu^{3+} phosphor in continuous supercritical water system. *J. Supercrit. Fluids*, 2007, **40**, 389–396.
18. Zhang, X. D., Liu, H., He, W., Wang, J. Y., Li, X. and Boughton, R. I., Novel synthesis of YAG by solvothermal method. *J. Cryst. Growth*, 2005, **275**, e1913–e1917.
19. Li, X., Liu, H., Wang, J. Y., Cui, H. M. and Han, F., Production of nano-sized YAG powders with spherical morphology and nonaggregation via a solvothermal method. *J. Am. Ceram. Soc.*, 2004, **87**, 2288–2290.
20. Cabañas, A., Li, J., Blood, P., Chudoba, T., Lojkowski, W., Poliakoff, M. *et al.*, Synthesis of nanoparticulate yttrium aluminum garnet in supercritical water–ethanol mixtures. *J. Supercrit. Fluids*, 2007, **40**, 284–292.
21. Yanagitani, T., Yagi, H. and Hiro, Y., Jpn. Pat., No. 10-101411, 1998.
22. Chen, Z. H., Yang, Y., Hu, Z. G., Li, J. T. and He, S. L., Synthesis of highly sinterable YAG nanopowders by a modified co-precipitation method. *J. Alloys Compd.*, 2007, **433**, 328–331.
23. Li, X., Li, Q., Wang, J. Y., Yang, S. L. and Liu, H., Synthesis of Nd^{3+} doped nano-crystalline yttrium aluminum garnet (YAG) powders leading to transparent ceramic. *Opt. Mater.*, 2007, **29**, 528–531.
24. Matsushita, N., Tsuchiya, N., Nakatsuka, K. and Yanagitani, T., Precipitation and calcination process for yttrium aluminum garnet precursors synthesized by the urea method. *J. Am. Ceram. Soc.*, 1999, **82**, 1977–1984.
25. Sordelet, D. J., Akinc, M., Panchula, M. L., Han, Y. and Han, M. H., Synthesis of yttrium aluminum garnet precursor powders by homogeneous precipitation. *J. Eur. Ceram. Soc.*, 1994, **14**, 123–130.
26. Zhou, Y. H., Lin, J., Yu, M., Han, S. M., Wang, S. B. and Zhang, H. J., Morphology control and luminescence properties of YAG:Eu phosphors prepared by spray pyrolysis. *Mater. Res. Bull.*, 2003, **38**, 1289–1299.
27. Kang, Y. C., Lenggoro, I. W., Park, S. B. and Okuyama, K., YAG:Ce phosphor particles prepared by ultrasonic spray pyrolysis. *Mater. Res. Bull.*, 2000, **35**, 789–798.
28. Kakade, M. B., Ramanathan, S. and Ravindran, P. V., Yttrium aluminum garnet powders by nitrate decomposition and nitrate–urea solution combustion reactions—a comparative study. *J. Alloys Compd.*, 2003, **350**, 123–129.

29. Fu, Y. P., Preparation of $Y_3Al_5O_{12}$:Ce powders by microwave-induced combustion process and their luminescent properties. *J. Alloys Compd.*, 2006, **414**, 181–185.
30. Ramanathan, S., Kakade, M. B., Roy, S. K. and Kutty, K. K., Processing and characterization of combustion synthesized YAG powders. *Ceram. Int.*, 2003, **29**, 477–484.
31. Xu, G. G., Zhang, X. D., He, W., Liu, H., Li, H. and Boughton, R. I., Preparation of highly dispersed YAG nano-sized powder by co-precipitation method. *Mater. Lett.*, 2006, **60**, 962–965.
32. Xu, G. G., Zhang, X. D., He, W., Liu, H. and Li, H., The study of surfactant application on synthesis of YAG nano-sized powders. *Powder Technol.*, 2006, **163**, 202–205.
33. Stengl, V., Bakardjieva, S., Subrt, J. and Szatmary, L., Titania aerogel prepared by low temperature supercritical drying. *Microporous Mesoporous Mater.*, 2006, **91**, 1–6.
34. Kocon, L., Despetis, F. and Phalippou, J., Ultralow density silica aerogels by alcohol supercritical drying. *J. Non-Cryst. Solids*, 1998, **225**, 96–100.
35. Weibel, G. L. and Ober, C. K., An overview of supercritical CO_2 applications in microelectronics processing. *Microelectron. Eng.*, 2003, **65**, 145–152.
36. Li, X., Liu, H., Wang, J. Y., Zhang, X. D. and Cui, H. M., Preparation and properties of YAG nano-sized powder from different precipitating agent. *Opt. Mater.*, 2004, **25**, 407–412.
37. Rosario, G. D., Ohara, S., Mancic, L. and Milosevic, O., Characterisation of YAG:Ce powders thermal treated at different temperatures. *Appl. Surf. Sci.*, 2004, **238**, 469–474.
38. Zhu, Y. H., Li, C. Z. and Hu, L. M., Mechanism of micropore disappearing in the later period of a-FeOOH dehydration. *J. East Chin. Univ. Sci. Technol.*, 1995, **21**, 567–568.
39. Tan, J. R., Shen, L. Z., Fu, X. S., Hou, W. X. and Chen, X. Z., Preparation of nanometer-sized $(1-x)\ SnO_2{\cdot}xSb_2O_3$ conductive pigment powders and the hydrolysis behavior of urea. *Dyes Pigments*, 2004, **61**, 31–38.
40. Su, J., Zhang, Q. L., Gu, C. J., Sun, D. L., Wang, Z. B., Qiu, H. L. *et al.*, Preparation and characterization of $Y_3Al_5O_{12}$ (YAG) nano-powder by co-precipitation method. *Mater. Res. Bull.*, 2005, **40**, 1279–1285.
41. Li, J., Pan, Y. B., Qiu, F. G., Wu, Y. S., Liu, W. B. and Guo, J. K., Synthesis of nanosized Nd:YAG powders via gel combustion. *Ceram. Int.*, 2007, **33**, 1047–1052.
42. Wang, J. Q., Xu, H. Y., Wang, Y. and Yue, Y. L., Effect of sulfate ions on YAG powders synthesized by microwave homogeneous precipitation. *J. Rare Earth*, 2006, **24**, 284–287.
43. Sato, T., Imaeda, S. and Sato, K., Thermal transformation of yttrium hydroxides to yttrium oxides. *Thermochim. Acta*, 1988, **133**, 79–85.
44. Sato, T., Thermal decomposition of aluminum hydroxides to aluminas. *Thermochim. Acta*, 1985, **88**, 69–84.
45. Antunes, M. L. P., Santos, H. S. and Santos, P. S., Characterization of the aluminum hydroxide microcrystals formed in some alcohol–water solutions. *Mater. Chem. Phys.*, 2002, **76**, 243–249.
46. Nien, Y. T., Chen, Y. L., Chen, I. G., Hwang, C. S., Su, Y. K., Chang, S. J. *et al.*, Synthesis of nano-scaled yttrium aluminum garnet phosphor by co-precipitation method with HMDS treatment. *Mater. Chem. Phys.*, 2005, **93**, 79–83.
47. Hirano, M. and Kato, E., Hydrothermal synthesis of nanocrystalline cerium (IV) oxide powders. *J. Am. Ceram. Soc.*, 1999, **82**, 786–788.
48. Dean, John A., *Inorganic Chemistry* (*12th ed.*). Lange's handbook of chemistry, New York, 1979, pp. 7–12.
49. Shi, J. L., Gao, J. H. and Lin, Z. X., Formation of monosized spherical aluminum hydroxide particles by urea method. *Solid State Ionics*, 1989, **32/33**, 537–543.
50. Apte, P., Burke, H. and Pickup, H., Synthesis of yttrium aluminum garnet by reverse strike precipitation. *J. Mater. Res.*, 1992, **7**, 706–711.
51. Eeckhaut, L., Verbeek, F., Deelstra, H. and Hoste, J., The stability of some lanthanide complexes with methylethyl glycolate and with methylpropyl glycolate. *Anal. Chim. Acta*, 1964, **30**, 369–376.
52. Hüttl, R., Bohmhammel, K., Wolf, G. and Oehmgen, R., Calorimetric investigations into enzymatic urea hydrolysis. *Thermochim. Acta*, 1995, **250**, 1–12.
53. Sordelet, D. and Akinc, M., Preparation of spherical, monosized Y_2O_3 precursor particles. *J. Colloid Interface Sci.*, 1988, **122**, 47–59.
54. Sun, Y., Qi, L., Lee, M., Lee, B. I., Samuels, W. D. and Exarhos, G. J., Photoluminescent properties of Y_2O_3:Eu^{3+} phosphors prepared via urea precipitation in non-aqueous solution. *J. Lumin.*, 2004, **109**, 85–91.
55. Li, J. G., Ikegami, T., Lee, J. H., Mori, T. and Yajima, Y., Co-precipitation synthesis and sintering of yttrium aluminum garnet (YAG) powders: the effect of precipitant. *J. Eur. Ceram. Soc.*, 2000, **20**, 2395–2405.
56. DeWith, G., Preparation, microstructure and properties of $Y_3Al_5O_{12}$ ceramics. *Philips J. Res.*, 1987, **42**, 119–130.
57. Hay, R. S., Phase transformation and microstructure evolution in sol-gel derived yttrium-aluminum garnet films. *J. Mater. Res.*, 1993, **8**, 578–604.
58. Nyman, M., Caruso, J. and Hampden-Smith, M. J., Comparison of solid-state and spray-pyrolysis synthesis of yttrium aluminate powders. *J. Am. Ceram. Soc.*, 1997, **80**, 1231–1238.
59. Novak, Z., Knez, Z., Ban, I. and Drofenik, M., Synthesis of barium titanate using supercritical CO_2 drying of gels. *J. Supercrit. Fluids*, 2001, **19**, 209–215.
60. Yin, S., Fujishiro, Y., Uchida, S. and Sato, T., Characterization of ceria and yttria co-doped zirconia/alumina composites crystallized in supercritical methanol. *J. Supercrit. Fluids*, 1998, **13**, 363–368.
61. Weibel, G. L. and Ober, C. K., An overview of supercritical CO applications in microelectronics processing. *Microelectron. Eng.*, 2003, **65**, 145–152.
62. Hu, Z. S., Wang, L. G., Ou, Z. W., Huang, L., Lai, R., He, T. *et al.*, Preparation of aerogel beryllium borate with supercritical carbon dioxide drying. *Powder Technol.*, 2001, **114**, 163–167.